Red-emitting gold nanoclusters for rapid fluorescence sensing of tryptophan metabolites

Ditta Ungor [a], Krisztián Horváth [a], Imre Dékány [a], Edit Csapó [a,b*]

[a] University of Szeged, Interdisciplinary Excellence Centre, Department of Physical Chemistry and Materials Science, H-6720 Rerrich B. square 1, Szeged, Hungary

[b] MTA-SZTE Biomimetic Systems Research Group, Department of Medical Chemistry, University of Szeged, H-6720 Dóm square 8, Szeged, Hungary

[*]Corresponding author: Edit Csapó (*E-mail address*: juhaszne.csapo.edit@med.u-szeged.hu)

Abstract

In this work, we first present a simple "green" preparation procedure of red-emitting ($\lambda_{emission}$ = 645 nm, d=1.5 ± 0.3 nm) fluorescent gold nanoclusters (Au NCs) using only γ-globulin (γG) immunoprotein as reducing and stabilizing agent. The γG-Au NCs are potent candidate for rapid detection of $_L$-kynurenine (Kyn) which is a dominant molecule of the kynurenine pathway (KP) of the tryptophan (Trp) metabolism. Sensing of Kyn has been carried out in phosphate buffer (PBS) solution and in artificial cerebrospinal fluid (aCSF) with the calculated detection limit of 15 and 22 μM, respectively. Beyond the definition of the dynamic range of 15-100 μM and analytical parameters (K_{SV}, k_0, k_q) the nature as well as the proposed mechanism of the quenching process was also suggested based on temperature-dependent spectrofluorometric studies. Moreover, a paper-based sensor technology was also successfully developed for rapid detection of Kyn with 5 μM detection limit.

Keywords: gold nanoclusters, γ-globulin, fluorescence detection, $_L$-kynurenine

1. Introduction

In the human body, the one of the major catabolic route of $_L$-Trp is the KP, which has an important role in several vital processes [1,2]. The intermediate molecules show neurotoxic (*e.g.* quinolinic acid) or neuroprotective (*e.g.* picolinic acid) features [3,4]. The discrepancy in the concentrations of these molecules from the standard values contributes to the emergence of neurodegenerative or psychiatric dysfunctions such as Alzheimer diseases, amyotrophic lateral sclerosis or schizophrenia [5–7]. So the strict monitoring of the KP is of the paramount importance in medicine. The simple body fluid-based quick optical tests cannot compete with the detection limit (LOD) of high-performance analytical techniques [8], but the developing of these simple probes for clinical use can greatly facilitate to start the fast and specific therapeutics of the patients on time. So far, only a few experimental results have been published regarding optical phenomena-based detection of the KP metabolites. J. Klockow *et al.* presented the sensing of Kyn using a coumarin aldehyde sensor, which enhanced the fluorescence of the Kyn but it can only be used in extreme acidic (pH ~ 1) condition [9]. T. Kaper *et al.* occupied a fluorescent fusion-protein nanosensor as a "turn-off" Trp quencher, but the protein was produced by a relative complex and expensive genetic engineering method [10]. Based on the localized surface plasmon resonance (LSPR) phenomena, the noble metal NPs have a well-known size-, composition- and shape-dependent individual optical properties [11,12] which are widely used for development of effective and rapid sensors. The shape and size of NPs can be systematically tuned by means of the synthesis conditions or the quality and the quantity of the reducing and stabilizing agents. Biomolecules such as peptides, amino acids, nucleotides, *etc*. are suitable for the direct reduction of gold ions as well as the stabilization of Au NPs and Au NCs [13–17]. The weight or molar ratios of the gold ions and the biomolecules have dominant role on the size and the optical feature of the nano-products. Generally, for sub-nanometer Au NCs a large excess of biomolecules is applied during the

reduction, which prevents the association of the locally reduced metal seeds by steric stabilization. The sensor application of the Au NCs is usually based on the quenching or enhancing of their fluorescence [18]. By quenching, several small biomolecules (*e.g.* dopamine or glucose) have already been detected using bovine serum albumin (BSA)- [19] or cysteine-directed Au NCs [20], respectively. Based on these findings, in this work γG-directed synthesis of red-emitting Au NCs have been presented, because this protein is not used previously for preparation of nano-objects. After the characterization, a method for the rapid detection of Kyn in PBS and in aCSF was developed. Several analytical and thermodynamic parameters were determined, which strongly support the nature and the mechanism of the quenching. Moreover, a simply paper-based drip sensor was also presented, which is possible use as a simple probe for clinical use.

2. Experimental

2.1. Materials

Gamma globulin from bovine blood (γG, 99%), gold(III) chloride acid trihydrate ($HAuCl_4 \times 3H_2O$, 99.9%), *L*-Trp ($C_{11}H_{12}N_2O_7$, 98%), kynurenic acid ($C_{10}H_7NO_3$, 98%), *L*-Kyn ($C_{10}H_{12}N_2O_3$, 98%), 3-hydroxy-*L*-kynurenine ($C_{10}H_{12}N_2O_4$, 98%), xanthurenic acid ($C_{10}H_7NO_4$, 96%), anthranilic acid (2-$(H_2N)C_6H_4CO_2H$, 98%), 3-hydroxyanthranilic acid ($HOC_6H_3(NH_2)CO_2H$, 97%), picolinic acid ($C_6H_5NO_2$, 99%), quinolinic acid ($C_7H_5NO_4$, 99%), nicotinamide-adenine-dinucleotide ($C_{21}H_{27}N_7O_{14}P_2$, 97%) were obtained from Sigma-Aldrich. Sodium hydroxide (NaOH, 99%), hydrochloric acid (HCl, 37%), sodium chloride (NaCl, 98%), potassium chloride (KCl, 96%), potassium phosphate monobasic (KH_2PO_4, 99 %), sodium hydrogen carbonate ($NaHCO_3$, 98%), D-glucose ($C_6H_{12}O_6$, 98%), calcium chloride ($CaCl_2$, 98%), magnesium chloride ($MgCl_2$, 99%) were provided from Molar. All of the chemical reagents were analytical grade and were used without further purification. The fresh stock solutions were prepared by using Milli-Q ultrapure water (18.2 MΩ·cm at 25 ºC)

in every cases. The concentration of the salts and compounds of the aCSF are the following: 127 mM NaCl, 1.0 mM KCl, 1.2 mM KH_2PO_4, 26 mM $NaHCO_3$, 10 mM D-glucose, 2.4 mM $CaCl_2$, 1.3 mM $MgCl_2$. The pH and the oxygen level are stabilized by bubbling with carbogen (95 % O_2 and 5 % CO_2).

2.2. Synthesis of γG-Au NCs

1.0 mL of 5.3 mM $HAuCl_4$ solution (m_{Au} =1.0 mg) was mixed in one-step with 5.0 mL γG aqueous solution, which includes 15 mg γG. After 15 min stirring 0.4 mL of 1 M NaOH solution was added to the mixture adjusting the final pH to 12. The reaction was undisturbed for 24 hours at 37 °C. The final product was purified by dialysis for 24 hours using cellulose dialysis tube with 12-14 kDa cut-off.

2.3. Instruments for characterization

The fluorescence spectra of the NCs were recorded on Jobin Yvon Fluoromax-4 spectrofluorometer (Horiba) using excitation wavelength at 350 nm with 3 nm slit in a 1 cm quartz cuvette. The lifetime and the quantum yield (QY%) were determined by the Edinburgh Instruments FLS920 time-resolved photoluminescence (PL) spectrometer. The wavelength of the excitation was 378 nm and the cresyl violet served as reference. The Fourier transform infrared (FT-IR) spectroscopy studies were performed by using Digilab Division FTS-65A/896 Fourier Transform infrared spectrometer (BIO-RAD) with a Harrick's Meridian® SplitPea single-reflection diamond attenuated total reflectance (ATR) accessory. All IR spectra were registered at 4 cm^{-1} optical resolution by averaging 256 interferrograms. The Circular Dichroism (CD) measurements were carried out using JASCO J-1100 CD spectrometer (ABL&JASCO, Hungary) between 300-180 nm. The Reed model [21] was used to assign the main secondary structural elements of the protein. The hydrodynamic diameters were determined with a Zetasizer Nano ZS ZEN 4003 apparatus (Malvern Inst., UK) equipped with a He-Ne laser (λ = 633 nm) at 25 ± 0.1 °C. The HRTEM images were taken on

Tecnai G2 instrument using 220 kV accelerating voltage and the images were analyzed with ImageJ software based on the average diameter of 150 particles. The X-ray photoelectron spectroscopy (XPS) measurements were done by SPECS instrument equipped with a PHOIBOS 150 MCD 9 hemispherical analyzer to confirm the oxidation state of gold. The thermometric titrations were performed using a MicroCal VP-ITC (Isothermal Titration Calorimeter, MicroCal, USA) power compensation microcalorimeter with a cell volume of 1.4301 mL. The enthalpy changes were recorded upon stepwise additions of Kyn into the reaction cell containing γG from a 300 μL syringe. Aliquots of 15 mL were injected at periodic time intervals (10 s per injection, 5 min between injections). Blank experiments were done in order to make corrections for the enthalpy changes corresponding to dilution of titrant. The calorimeter power signals were evaluated with Origin® 7 software supplied by Microcal.

2.4. Detection procedures of the tryptophan metabolites

250-250 μL of purified γG-Au NCs (c_{Au} = 0.05 mM) were pipetted into an aqueous solution, which contained the different test molecules in similar concentrations (c = 1 mM) in PBS and aCSF solution in order to better model the chemical environment within the human body. The final volume was 5 mL. In case of Kyn detection the PL quenching studies was carried out in the concentration range of 1 nM - 1 mM and at 298, 303, 308 and 313 K temperatures. The PL spectrum of the γG-Au NCs solution was registered as reference in every cases to define the I_0/I values.

3. Results and discussion

3.1. Effect of synthesis conditions and characterization of the prepared γG-Au NCs

The ratio of the $AuCl_4^-$ ions and the protein has a great influence to the size and the optical properties of the final products. Many ratios of γG:$AuCl_4^-$ from 1:1 to 125:1 have been tested in order to find optimal conditions for the preparation of stabile nanosized products. It was

established that under the same conditions (pH, temperature, reaction time) the systematic change in the ratios of the reactants results in the formation of both Au NPs and Au NCs. Namely, at γG:$AuCl_4^-$/1:1 weight ratio, colloidal Au NPs were formed with a characteristic plasmon band at 525 nm (**Fig. S1A**) [22]. An average size of 24.2 ± 12.3 nm is proved by TEM (**Fig. S1B**). Increase in γG:$AuCl_4^-$ weight ratio from 1:1 to 2:1 results in the disappearance of the plasmon band and a characteristic emission band is evolved in the emission spectra at 645 nm. The most intensive red fluorescence is detected at γG:$AuCl_4^-$/15:1 weight ratio, but further increase in the protein excess results in the decrease in the fluorescence intensities (**Fig. S2A)**. As **Fig. S2B** shows the optimal synthesis time of 24 hours, where the fluorescence intensity reaches the maximum value. Using the above mentioned optimal parameters the γG-Au NCs were successfully synthesized. A typical emission spectrum of the NCs can be seen on the **Fig. 1A.**

(Here Figure 1)

The estimated PL lifetime of 1.2 μs and the QY(%), which is 4.4 %, indicates the formation of the few nanometer Au NCs [18]. The XPS spectra were recorded before (**Fig. S3A**) and after (**Fig. 1B**) dialysis in order to confirm the successful purification of the clusters. The binding energies were detected at Au $4f_{7/2}$ = 84.5 eV and $4f_{5/2}$ = 88.2 eV. The peak maximum of $4f_{7/2}$ is located at ~84 eV in case of bulk gold but the decrease in the size of the gold particles results in a shift of the peak to 84.2–84.8 eV [23], which is in good agreement with our experiments. It can be seen that the sample predominantly contains Au^0 in the cluster cores after cleaning. Although, before dialysis the initial $AuCl_4^-$ also presents in a few percent with the peak maxima at Au(III) $4f_{7/2}$ = 86.3 eV and Au(III) $4f_{5/2}$ = 89.8 eV. The size and the hydrodynamic diameter of Au NCs can be defined by HRTEM images (**Fig. 2A**) and DLS, where 1.5 ± 0.3 nm and 4.4 ± 0.5 nm of average size was proved, respectively.

(Here Figure 2)

The kinetic stability of the cluster dispersion was investigated by DLS and ζ-potential measurements (**Fig 2B**). As it can be seen that, the average hydrodynamic diameter shows outstandingly high value (d ~ 400 nm) at pH ~ 5 as well as the ξ-potential also reaches the zero value, which refers the aggregation of the clusters. The reason for aggregation is presumably that the pH ~ 5 corresponds to the isoelectric point (pI = 4.6-6.5) for the immunoglobulin G (IgG) which is the main fraction of γG. At this pH the precipitation of this protein occurs since the IgG is an isolable protein [24,25]. **Fig. 2B** clearly shows that there is no significant change in the hydrodynamic diameter and the ξ-potential value at around physiological pH (pH 7.4) as well as the intensity of the emission band at 645 nm (**Fig. S3B**) does not change either indicating in high kinetic stability of the clusters.

The secondary protein structure of γG has been studied by FT-IR (**Fig. S4**) and CD studies (**Fig. S5**) to get structural information on the protein before and after synthesis. In the FT-IR spectra the Amide I band was detected at 1633 cm^{-1} and 1630 cm^{-1}, while the position of the Amide II band was identified at 1531 cm^{-1} and 1562 cm^{-1} in the γG and the γG-Au NCs, respectively. The ratio of the ordered β-sheets decreases from *ca*. 48% to 28 % and an extended structure which contains β-turns (17%) the random coil (*ca.* 53%) becomes determinative [26]. Both the shift of the Amide bands as well as the change of the ratio of the secondary structural elements of the protein (**Table S1**) supports that under physiological conditions the subnanometer-sized gold seed are inserted into the protein chains. During the synthesis, the partial reduction of the gold(III) ions primarily eventuated along the side chain of the tyrosine (Tyr) and tryptophan (Trp) amino acid in the used protein. Following a "chain migration", the gold(I) ions are trapped along the sulfur-containing amino acids, where the further reduction is occurred and the final cluster seeds are formed. This "chain migration"

and seed inclusion causes the unfolding of the protein chain, which reduces the amount of the β sheets in the applied protein after the clusters are formed [27,28].

3.2. Rapid fluorescence sensing of Trp metabolites

The fluorescence of Au NCs strongly depends on the chemical environment [29,30] and the enhancing or the quenching of the luminescence of the clusters have been occurred in the presence of different analytes. In this work, the detection of the ten dominant metabolites of the KP (**Fig. S6**) has been carried out in PBS and aCSF; the names of the metabolites are seen on **Fig. 3B**. As **Fig. 3 and Fig S7A show**, the quenching of the fluorescence was observed in case of the Kyn (2) dominantly.

(Here Figure 3)

The anthranilic acid (6) has intensive blue fluorescence [31], which can overlap with the red emission of the Au NCs but the deconvolution of the emission spectrum indicated that the quenching is not occurred in the presence of this molecule. The monitoring of the Kyn concentration is an important task in medical diagnostics. The increase of the Kyn concentration in the human body can refer to the neopterin-catalyzed dissimilation of Trp by the indoleamine 2,3-dioxygenase (IDO) [32]. The increased IDO-activity correlates with tumor progression in various cancer diseases because presumably the IDO is accountable for the hiding the tumor cells from the immune systems [32–34]. Due to this decisive selectivity, the NCs can be potentially utilized for tracking the Kyn and can be conducive to early detection of many lethal disorders. Based on the commonly used publication of H. P. Loock and P. D. Wentzell [35] the LOD of 15 μM (in PBS) and 22 μM (in aCSF) was calculated which is somewhat larger value than the smallest, experimentally detectable amount of Kyn (c ~1 μM, **Fig. S7B**) in both medium. Taking into account the exact concentration of the Kyn in human liquor (*ca*. 3 μM) or in serum (*ca*. 6-8 μM) in case of several cancer diseases [33,36] our synthesized nano-system is potentially suitable for a rapid detection of Kyn. The dynamic

range was appointed between 15-100 μM (**Fig. S8**) based on the PL studies. Comparison of the LOD of the Kyn by using different analytical techniques and an optical sensor is summarized in **Table S2**.

3.3. Physicochemical interpretation of the interaction between γG-Au NCs and Kyn

In addition to the main analytical parameters, the thermodynamic state functions were also determined. In the linear range, the quenching tests have been performed at 298, 303, 308 and 313 K to interpret the possible mechanism of the quenching [37]. Based on the Stern-Volmer equation (**Eq. 1.**) the measurement data were depicted. The Stern-Volmer representation includes the $\boldsymbol{I_0}$ and $\boldsymbol{I}$, which are the maximum of the fluorescence intensity before and after addition of Kyn. The $\boldsymbol{K_{SV}}$ is the Stern-Volmer quenching constant and the $\boldsymbol{[Q]}$ is the equilibrium concentration of Kyn.

$$I_0/_I = 1 + K_{SV}[Q] = 1 + k_q * \tau_0[Q] \quad (1)$$

The linearity of the Stern-Volmer representation suggests that, the combined quenching was unlikely; only dynamic or static quenching is probable in the examined linear range (**Fig. 4A**).

(Here Figure 4)

The behavior of the K_{SV} was investigated depending on the temperature (**Fig. S9**). It was found that, the K_{SV} is increased in the raising of the temperature, which supports the dynamic quenching between 15-100 μM of c_{Kyn}. In case of the dynamic or collision quenching, the K_{SV} can be given as the product of the bimolecular quenching rate constant ($\boldsymbol{k_q}$) and the measured fluorescence lifetime of the fluorophore in the absence of the quencher ($\boldsymbol{\tau_0}$). In order to discovery of the factors, which influence on the rate of the collision quenching, it was important to determine the values of the diffusion-controlled bimolecular quenching rate constant ($\boldsymbol{k_0}$) depending on the temperatures. This constant can be given by using the Smoluchowski equation (**Eq. 2.**), where the $\boldsymbol{r_f}$ and $\boldsymbol{r_q}$ are the average hydrodynamic diameter

of the fluorophore and the quencher, the $\boldsymbol{D_f}$ and $\boldsymbol{D_q}$ are the diffusion coefficients of the fluorophore and the quencher.

$$k_0 = {}^{4\pi N}/_{1000} * (r_f + r_q)(D_f + D_q) \quad (2)$$

The $\boldsymbol{N}$ is the Avogadro's number and the molarity was transformed into molecules/mL by expressing N/1000. The diffusion coefficients of the reactant can be calculated by the Stokes-Einstein equation (**Eq. 3.**).

$$D = {}^{kT}/_{6\pi\eta r} \quad (3)$$

The diffusion coefficient depends on the measured temperature ($\boldsymbol{T}$), the dynamic viscosity of the medium ($\boldsymbol{\eta}$) and the hydrodynamic diameter of the particle ($\boldsymbol{r}$). The $\boldsymbol{k}$ is the Boltzmann constant. The average hydrodynamic diameter of 4.4 nm is used based on DLS results. In case of the Kyn, the parameters were calculated using $\boldsymbol{r_q}$ = 1.65 nm based on the PubChem (Open Chemistry Database, CID 161166). The results of the Stern-Volmer evaluations and the calculations are summarized in **Table 1.** The values of k_q and k_0 and their ratios provide more information on the quenching mechanism.

(Here Table 1)

The quenching is diffusion-driven, when the k_q value is around 1×10^{10} $M^{-1}s^{-1}$. The k_q has nearly similar magnitude as the value for diffusion-controlled reaction ($k_q < k_0$ at all the measured temperatures). This fact refers a steric inhibition, which is attributable to the protein shell on the cluster surface [38]. To further support of the dynamic quenching, additional studies were also performed using BSA and lysozyme (LYZ)-stabilized red-emitting Au NCs, which was synthesized in our lab previously. Regardless of the protein we established that the quenching has been similarly occurred by the Kyn which indicates the gold-specific particularity of the Kyn-Au NCs interaction. In these control samples the LOD was measurable higher (*ca.* 40 µM), so these results were not discussed in detail. In support of this

result, ITC measurements have also been carried out. The enthalpograms, which were recorded during the interaction of the γG and Kyn, did not show any measurable heat effect after the extraction of the background signal. During the collision quenching, the K_{SV} represents a combined process, which can be describable by this general scheme (**Eq. 4**):

$$Au\ NCs^* + Kyn \rightleftharpoons [Au\ NCs - Kyn]^{\ddagger} \longrightarrow Au\ NCs + Kyn^*. \quad (4)$$

The part processes have own rate constants. These individual steps are the formation of the activated complex ([Au NCs-Kyn]‡) resulting from the collision (**k_1**) and the decomposition of the activated complex to the ground-state fluorophore and excited quencher with energy transfer (**k_2**) or its non-reactive disintegration (**k'_1**). In consequence, the K_{SV} can be used as an equilibrium constant based on this generally accepted definition: $K_{SV} = {(k'_1 + k_2)}/{k_1}$.

Accordingly, the thermodynamic parameters can be determined using the integrated van't Hoff equation (**Eq. 5.**) [39].

$$\ln K_{SV} = -{\Delta H^0(T^0)}/{RT} + {\Delta S^0(T^0)}/{R} + {\Delta C_p}/{R}\left[\left({(T - T^0)}/{T}\right) - \ln\left({T}/{T^0}\right)\right] \quad (5)$$

In case of the commonly used linear regression, the calculated coefficient was 0.954 while the application of the non-linear parameter estimation caused better alignment with the correlation coefficient of 0.991 (**Fig. 4B.**). The Gibbs free energy change (ΔG) was given by the $\Delta G = \Delta H^0 - T\Delta S^0$ equation. The calculated thermodynamic data can be seen in **Table 2**.

(Here Table 2)

The negative value of the ΔG (*ca.* -22 kJ mol^{-1}) refers that, the interaction between the γG-Au NCs and Kyn is thermodynamically favorable. Since the standard enthalpy change (ΔH^0) is positive, the quenching is endotherm and the quenching between the reactants occurs via a charge transfer process [40]. This charge transfer presumably can be an excited electron-

induced acidic proton transfer from the Kyn to the protein shell of the Au NCs such as in case of the BSA-Au NCs/dopamine sensor [41]. Furthermore, the kynurenic acid and the 3-hydroxy-*L*-kynurenine have relatively similar chemical structure as the Kyn, slight quenching was also appreciable in case of these molecules. As the absolute value of the entropy member is greater than the enthalpy member at all measured temperatures ($|T\Delta S^0| > |\Delta H^0|$) the quenching is presumably entropy-driven [37].

(Here Figure 5)

Promoting to develop of the Kyn sensitive clinical quick test, a paper-based example is demonstrated on the **Fig. 5**. The paper was sliced into 1×1 cm squares and 2.5 µL from the original concentrated Au NCs was dropped and dried on paper. This amount of the γG-Au NCs was enough to the rapid optical detection of 5 µM Kyn in aCSF solution (**Fig S10**) which is in good accordance with the toxic Kyn concentration of liquor and serum for several cancer (vulvar, ovarian cancer and leukemia) diseases.

4. Conclusion

A reproducible synthesis of Au NCs (λ_{em} = 645 nm, d = 1.5 ± 0.3 nm) has been presented in aqueous medium at 37 °C. During the cluster formation, the dominant changes in the secondary structural elements of the protein have been interpreted. The red-emitting NCs have been successfully used as the potential biosensor of Kyn with the calculated LOD of 15 and 22 µM in different medium. The dynamic quenching was obtained at several temperatures and we support that the quenching process is thermodynamically favorable, endothermic and entropy-controlled. Even, a charge transfer between the fluorophore and the quencher may occurs. For paper-based rapid test we established that only one small drop (2.5µL) is enough to rapidly detect the presence of 5 µM of Kyn in model human liquor which has important relevance for several cancer and neurological diseases.

Acknowledgement

The authors would like to thank to Péter Baranyai (MTA TTK, Budapest, Hungary) for the PL lifetime and QY(%) measurement. The research was supported by National Research, Development and Innovation Office-NKFIH through project K116323 and GINOP-2.3.2-15-2016-00038. This paper was supported by the UNKP-18-4 New National Excellence Program of the Ministry of Human Capacities. The Ministry of Human Capacities, Hungary grant 20391-3/2018/FEKUSTRAT is acknowledged.

5. References

[1] Y. Chen, G.J. Guillemin, Kynurenine pathway metabolites in humans: Disease and healthy states, Int. J. Tryptophan Res. 2 (2009) 1–19.

[2] J.P. Routy, B. Routy, G.M. Graziani, V. Mehraj, The kynurenine pathway is a double-edged sword in immune-privileged sites and in cancer: Implications for immunotherapy, Int. J. Tryptophan Res. 9 (2016) 67–77.

[3] Y. Chen, R. Stankovic, K.M. Cullen, V. Meininger, B. Garner, S. Coggan, R. Grant, B.J. Brew, G.J. Guillemin, The kynurenine pathway and inflammation in amyotrophic lateral sclerosis, Neurotox. Res. 18 (2010) 132–142.

[4] A. Zinger, C. Barcia, M.T. Herrero, G.J. Guillemin, The involvement of neuroinflammation and Kynurenine pathway in Parkinson's disease, Parkinsons. Dis. 2011 (2011).

[5] M.P. Heyes, K. Saito, J.S. Crowley, L.E. Davis, M.A. Demitrack, M. Der, L.A. Dilling, et al. Quinolinic acid and kynurenine pathway metabolism in inflammatory and non-inflammatory neurological disease, Brain. 115 (1992) 1249–1273.

[6] K. Schroecksnadel, S. Kaser, M. Ledochowski, G. Neurauter, E. Mur, M. Herold, D. Fuchs, Increased degradation of tryptophan in blood of patients with rheumatoid arthritis, J. Rheumatol. 30 (2003) 1935–1939.

[7] N. Muller, A.-M. Myint, M. J. Schwarz, Kynurenine Pathway in Schizophrenia: Pathophysiological and Therapeutic Aspects, Curr. Pharm. Des. 17 (2011) 130–136.

[8] C. Xiao, Y. Chen, X. Liang, Z. Xie, M. Zhang, R. Li, Z. Li, X. Fu, X. Yu, W. Shi, A modified HPLC method improves the simultaneous determination of plasma kynurenine and tryptophan concentrations in patients following maintenance hemodialysis, Exp. Ther. Med. 7 (2014) 907–910.

[9] J.L. Klockow, T.E. Glass, Development of a fluorescent chemosensor for the detection of kynurenine, Org. Lett. 15 (2013) 235–237.

[10] T. Kaper, L.L. Looger, H. Takanaga, M. Platten, L. Steinman, W.B. Frommer, Nanosensor detection of an immunoregulatory tryptophan influx/kynurenine efflux cycle, PLoS Biol. 5 (2007) 2201–2210.

[11] K.A. Willets, R.P. Van Duyne, Localized Surface Plasmon Resonance Spectroscopy and Sensing, Annu. Rev. Phys. Chem. 58 (2007) 267–297.

[12] E. Csapó, A. Oszkó, E. Varga, Á. Juhász, N. Buzás, L. Kőrösi, A. Majzik, I. Dékány, Synthesis and characterization of Ag/Au alloy and core(Ag)–shell(Au) nanoparticles, Colloids Surfaces A Physicochem. Eng. Asp. 415 (2012) 281–287.

[13] J.J. Feng, H. Huang, D.L. Zhou, L.Y. Cai, Q.Q. Tu, A.J. Wang, Peptide-templated synthesis of wavelength-tunable fluorescent gold nanoparticles, J. Mater. Chem. C. 1 (2013) 4720–4725.

[14] H. Li, J. Chen, H. Huang, J.J. Feng, A.J. Wang, L.X. Shao, Green and facile synthesis of l-carnosine protected fluorescent gold nanoclusters for cellular imaging, Sensors Actuators, B Chem. 223 (2016) 40–44.

[15] V. Hornok, E. Csapó, N. Varga, D. Ungor, D. Sebők, L. Janovák, G. Laczkó, I. Dékány, Controlled syntheses and structural characterization of plasmonic and red-emitting gold/lysozyme nanohybrid dispersions, Colloid Polym. Sci. 294 (2016) 49–58.

[16] H. Li, H. Huang, J.J. Feng, X. Luo, K.M. Fang, Z.G. Wang, A.J. Wang, A polypeptide-mediated synthesis of green fluorescent gold nanoclusters for Fe^{3+} sensing and bioimaging, J. Colloid Interface Sci. 506 (2017) 386–392.

[17] H. Li, H. Huang, A.J. Wang, H. Feng, J.J. Feng, Z. Qian, Simple fabrication of eptifibatide stabilized gold nanoclusters with enhanced green fluorescence as biocompatible probe for in vitro cellular imaging, Sensors Actuators, B Chem. 241 (2017) 1057–1062.

[18] J. Zheng, C. Zhou, M. Yu, J. Liu, Different sized luminescent gold nanoparticles, Nanoscale. 4 (2012) 4073–4083.

[19] B. Hemmateenejad, F. Shakerizadeh-Shirazi, F. Samari, BSA-modified gold nanoclusters for sensing of folic acid, Sensors Actuators, B Chem. 199 (2014) 42–46.

[20] A.M.P. Hussain, S.N. Sarangi, J.A. Kesarwani, S.N. Sahu, Au-nanocluster emission based glucose sensing, Biosens. Bioelectron. 29 (2011) 60–65.

[21] J. Reed, T.A. Reed, A Set of Constructed Type Spectra for the Practical Estimation of Peptide Secondary Structure from Circular Dichroism, Anal. Biochem. 254 (1997) 36–40.

[22] B. Streszewski, W. Jaworski, K. Pacławski, E. Csapó, I. Dékány, K. Fitzner, Gold nanoparticles formation in the aqueous system of gold(III) chloride complex ions and hydrazine sulfate-Kinetic studies, Colloids Surfaces A Physicochem. Eng. Asp. 397 (2012) 63–72.

[23] S. Peters, S. Peredkov, M. Neeb, W. Eberhardt, M. Al-Hada, Size-dependent XPS spectra of small supported Au-clusters, Surf. Sci. 608 (2013) 129–134.

[24] R.H. Pain, The molecular weights of the peptide chains of gamma-globulin, Biochem. J. 88 (1963) 234–9.

[25] A. Elkak, T. Yehya, I. Salloub, F. Berry, A one step separation of immunoglobulin G

from bovine serum by pseudobioaffinity chromatography on histidine grafted to epoxy activated sepharose, Biotechnol. Bioprocess Eng. 17 (2012) 584–590.

[26] A. Adochitei, G. Drochioiu, Rapid characterization of peptide secondary structure by FT-IR spectroscopy, Rev. Roum. Chim. 56 (2011) 783–791.

[27] X.L. Cao, H.W. Li, Y. Yue, Y. Wu, PH-Induced conformational changes of BSA in fluorescent AuNCs@BSA and its effects on NCs emission, Vib. Spectrosc. 65 (2013) 186–192.

[28] B.A. Russell, B. Jachimska, P. Komorek, P.A. Mulheran, Y. Chen, Lysozyme encapsulated gold nanoclusters: Effects of cluster synthesis on natural protein characteristics, Phys. Chem. Chem. Phys. 19 (2017) 7228–7235.

[29] J. Sun, Y. Jin, Fluorescent Au nanoclusters: Recent progress and sensing applications, J. Mater. Chem. C. 2 (2014) 8000–8011.

[30] M. Shellaiah, K. Sun, Luminescent Metal Nanoclusters for Potential Chemosensor Applications, Chemosensors. 5 (2017) 36.

[31] A.S. Culf, H. Yin, S. Monro, A. Ghosh, D.A. Barnett, R.J. Ouellette, M. Čuperlović-Culf, S.A. McFarland, A spectroscopic study of substituted anthranilic acids as sensitive environmental probes for detecting cancer cells, Bioorganic Med. Chem. 24 (2016) 929–937.

[32] S. Geisler, P. Mayersbach, K. Becker, H. Schennach, D. Fuchs, J.M. Gostner, Serum tryptophan, kynurenine, phenylalanine, tyrosine and neopterin concentrations in 100 healthy blood donors, Pteridines. 26 (2015) 31–36.

[33] R.A. De Jong, H.W. Nijman, H.M. Boezen, M. Volmer, K.A. Ten Hoor, J. Krijnen, A.G.J. Van Der Zee, H. Hollema, I.P. Kema, Serum tryptophan and kynurenine concentrations as parameters for indoleamine 2,3-dioxygenase activity in patients with endometrial, ovarian, and vulvar cancer, Int. J. Gynecol. Cancer. 21 (2011) 1320–1327.

[34] R. Mabuchi, T. Hara, T. Matsumoto, Y. Shibata, N. Nakamura, H. Nakamura, J. Kitagawa, et al. High serum concentration of L-kynurenine predicts unfavorable outcomes in patients with acute myeloid leukemia, Leuk. Lymphoma. 57 (2016) 92–98.

[35] H.P. Loock, P.D. Wentzell, Detection limits of chemical sensors: Applications and misapplications, Sensors Actuators, B Chem. 173 (2012) 157–163.

[36] D. Holmberg, E. Franzén-Röhl, R. Idro, R.O. Opoka, P. Bangirana, C.M. Sellgren, R. Wickström, A. Färnert, L. Schwieler, G. Engberg, C.C. John, Cerebrospinal fluid kynurenine and kynurenic acid concentrations are associated with coma duration and long-term neurocognitive impairment in Ugandan children with cerebral malaria, Malar. J. 16 (2017) 1–9.

[37] S. Al-Omari, Separation of static and dynamic thermodynamic parameters for the interaction between pyropheophorbide methyl ester and copper, J. Porphyr. Phthalocyanines. 18 (2014) 297–304.

[38] J.R. Lakowicz, Principles of Fluorescence Spectroscopy, Third, Springer US, Boston, MA, 2006.

[39] Á. Juhász, E. Csapó, D. Ungor, G.K. Tóth, L. Vécsei, I. Dékány, Kinetic and Thermodynamic Evaluation of Kynurenic Acid Binding to $GluR1_{270-300}$ Polypeptide by Surface Plasmon Resonance Experiments, J. Phys. Chem. B. 120 (2016) 7844–7850.

[40] M. Bordbar, M. Shamsipur, N. Alizadeh, Thermodynamics studies of fluorescence quenching and complexation behavior of thallium(I) ion with some polyazamacrocycles, J. Photochem. Photobiol. A Chem. 178 (2006) 83–89.

[41] S. Govindaraju, S.R. Ankireddy, B. Viswanath, J. Kim, K. Yun, Fluorescent Gold Nanoclusters for Selective Detection of Dopamine in Cerebrospinal fluid, Sci. Rep. 7 (2017) 1–12.

Figure Captions

Figure 1 (A) Fluorescence emission spectrum of γG-Au NCs with the photo of the γG:Au/15:1 aqueous sample under UV-lamp (m_{Au} = 1 mg, λ_{ex} = 350 nm). **(B)** XPS spectrum of the purified γG-Au NCs.

Figure 2 (A) Representative HRTEM image of the γG-Au NCs. **(B)** The hydrodynamic diameter (black points) and the ξ-potential values (gray points) of the γG-Au NCs as a function of pH.

Figure 3 (A) The photos of the γG-Au NCs dispersions under UV-lamp after addition of 1.0 mM of KP molecules (c_{Au} = 0.05 mM). **(B)** The relative fluorescence of the clusters in the presence of 1.0 mM test molecules.

Figure 4 (A) The Stern-Volmer fitting of the measured data based on the **Eq. 1** at 298 K with the chemical structure of Kyn. **(B)** The van't Hoff plot (gray line: linear fitting, black line: non-linear fitting) of the interaction between Kyn and γG-Au NCs.

Figure 5 The photos of the paper-based Kyn sensor under UV-lamp before (left) and after (right) addition of Kyn (c_{Kyn} = 5.0 μM).

Table 1 The Stern-Volmer constants ($\mathbf{K_{SV}}$) with the correlation coefficients ($\mathbf{R^2}$), the calculated bimolecular quenching rate constants ($\mathbf{k_q}$), the diffusion-controlled bimolecular quenching rate constants ($\mathbf{k_0}$) and the diffusion coefficients of the γG-Au NCs ($\mathbf{D_{NCs}}$) and the Kyn ($\mathbf{D_{Kyn}}$) at the measured temperatures.

Table 2 The Stern-Volmer constants ($\mathbf{K_{SV}}$) with the correlation coefficients ($\mathbf{R^2}$) and the defined thermodynamic parameters ($\Delta\mathbf{H°}$, $\Delta\mathbf{S°}$, $\Delta\mathbf{G}$) of the quenching process between γG-Au NCs and Kyn at the examined temperatures.

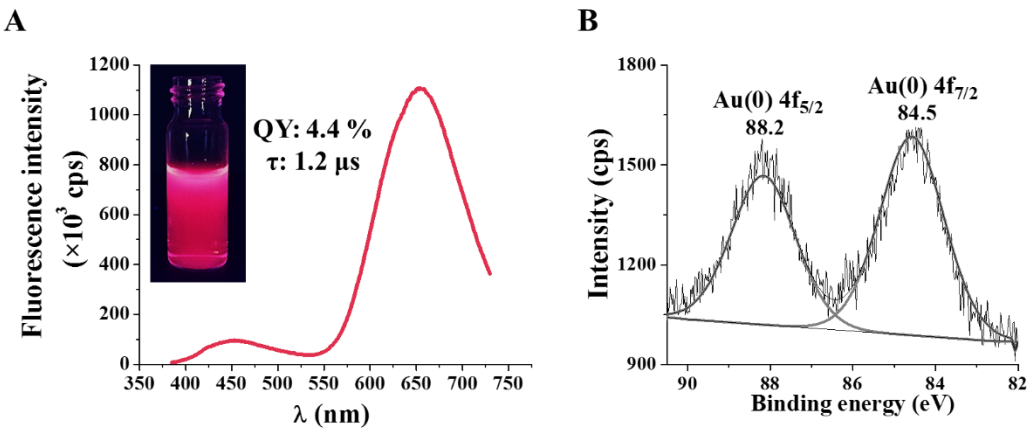
A
B
Fluorescence intensity
(×10³ cps)
QY: 4.4 %
τ: 1.2 µs
λ (nm)
Au(0) 4f5/2
88.2
Au(0) 4f7/2
84.5
Intensity (cps)
Binding energy (eV)

Figure 1

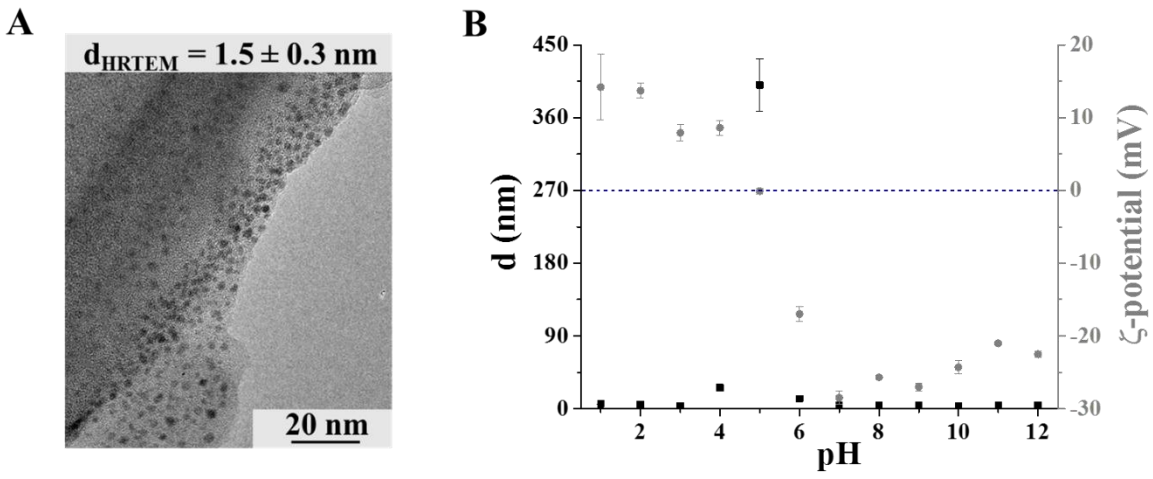
A
d_{HRTEM} = 1.5 ± 0.3 nm
20 nm
B
d (nm)
ζ-potential (mV)
pH
450
360
270
180
90
0
20
10
0
-10
-20
-30
2
4
6
8
10
12

Figure 2

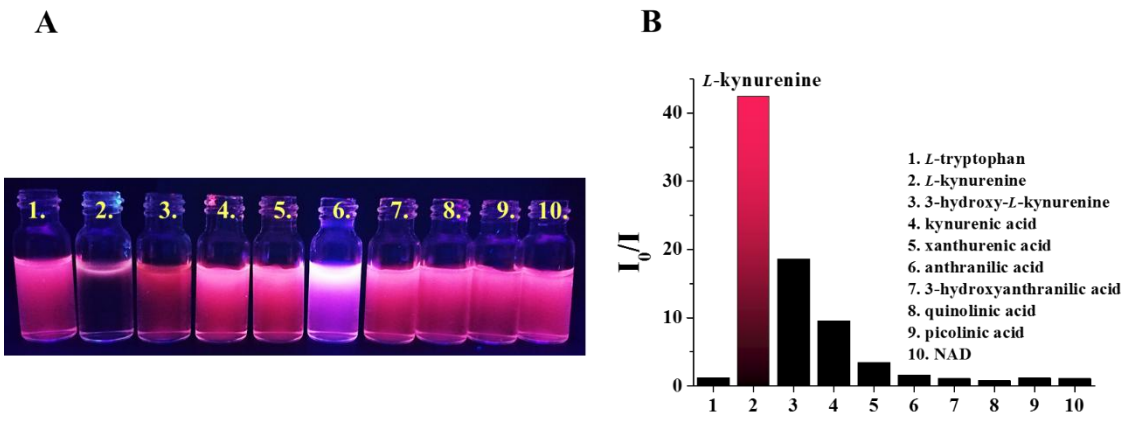
A
B
1.
2.
3.
4.
5.
6.
7.
8.
9.
10.
L-kynurenine
I0/I
40
30
20
10
0
1
2
3
4
5
6
7
8
9
10
1. L-tryptophan
2. L-kynurenine
3. 3-hydroxy-L-kynurenine
4. kynurenic acid
5. xanthurenic acid
6. anthranilic acid
7. 3-hydroxyanthranilic acid
8. quinolinic acid
9. picolinic acid
10. NAD

Figure 3

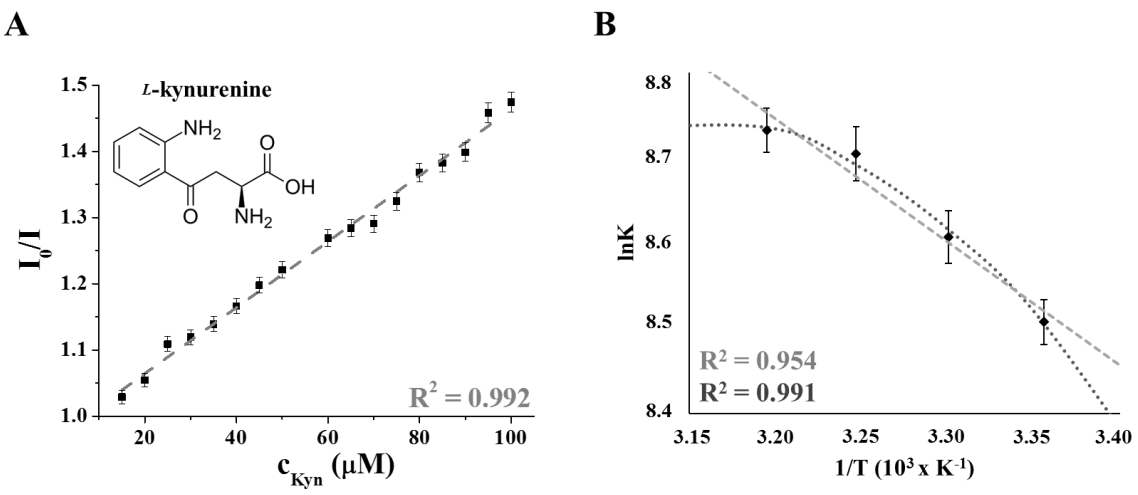
A
B
L-kynurenine
NH2
O
OH
O
NH2
I0/I
cKyn (μM)
R2 = 0.992
lnK
1/T (10³ x K⁻¹)
R2 = 0.954
R2 = 0.991

Figure 4

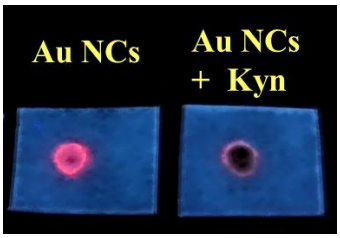

Figure 5

Table 1

T [K]	K_{SV} [M^{-1}]	R^2	k_q [$M^{-1}\ s^{-1}$]	k_0 [$M^{-1}\ s^{-1}$]	D_{NCs} [$cm^2\ s^{-1}$]	D_{Kyn} [$cm^2\ s^{-1}$]
298	4950 ± 130	0.992	$4.13\times10^{9} \pm 1.08\times10^{8}$	1.12×10^{10}	1.11×10^{-6}	4.22×10^{-6}
303	5470 ± 170	0.988	$4.56\times10^{9} \pm 1.42\times10^{8}$	1.27×10^{10}	1.26×10^{-6}	4.79×10^{-6}
308	6070 ± 140	0.992	$5.06\times10^{9} \pm 1.17\times10^{8}$	1.42×10^{10}	1.41×10^{-6}	5.33×10^{-6}
313	6220 ± 160	0.991	$5.18\times10^{9} \pm 1.33\times10^{8}$	1.61×10^{10}	1.60×10^{-6}	6.04×10^{-6}

Table 2

T [K]	K_{SV} [M^{-1}]	R^2	ΔH° [kJ mol^{-1}]	ΔS° [kJ mol^{-1} K^{-1}]	ΔG [kJ mol^{-1}]
298	4950 ± 130	0.992	14.16 ± 3.15	0.12 ± 0.01	-21.11
303	5470 ± 170	0.988			-21.71
308	6070 ± 140	0.992			-22.30
313	6220 ± 160	0.991			-22.89